ACS OMEGA

Article

Cite This: ACS Omega 2020, 5, 758−765

http://pubs.acs.org/journal/acsodf

Ionic Diffusion and Drug Release Behavior of Core−Shell-Functionalized Alginate−Chitosan-Based Hydrogel

Deepak Kumar Khajuria,*[,†,‡] Ramakrishna Vasireddi,[†,§] Manish Kumar Priydarshi,[†,§] and Debiprosad Roy Mahapatra*[,†]

[†]Laboratory for Integrative Multiscale Engineering Materials and Systems, Department of Aerospace Engineering, Indian Institute of Science, Bangalore 560012, India

[‡]Department of Orthopaedics and Rehabilitation, Center for Orthopaedic Research and Translational Science, The Pennsylvania State University College of Medicine, Hershey, Pennsylvania 17033, United States

ABSTRACT: This paper reports the core−shell structure effects in calcium alginate (CaALG) microbeads due to the threshold water level for phase transition and correlates these properties with respect to pH and electrical conductivity. Further, in this study, we used a novel microfluidic device for drug release testing to study the programmed release of risedronate (RIS-anti-osteoporotic drug) encapsulated in pH-responsive CaALG−chitosan (CHT) microbeads. Our microfluidic device contains a single straight microchannel containing a steplike barrier design used to restrict the mobility of the microbeads at the sample detection zone. For optical and fluorescence microscopy, single fluorescently labeled CaALG−CHT microbead containing RIS was placed in the sample detection zone by flowing through the inlet port with ultrapure water. The RIS release behavior from the microbeads at different pH (2.1, 4, 6.8, and 7.4) conditions was determined by using a spectrophotometer connected to the outlet port of the device. Results of our first study showed that the decrease in the concentration of $CaCl_2$ increases the swelling rate in CaALG microbeads. Maximum swelling was achieved with the lowest molar concentration of $CaCl_2$ used for fabrication of CaALG microbeads. Further, electrical current−voltage characteristic shows the nature of ionic mobility with respect to varying levels of pH indicating electrokinetic forces developed in the CaALG microbeads. By using a microfluidic device for drug release testing, we demonstrated that a sustained release delivery system for RIS can be prepared by coating with pH-sensitive and biodegradable CaALG−CHT. The CaALG−CHT microbeads used for encapsulating RIS are resistant to the acidic environment of the stomach. This may improve the therapeutic effectiveness and reduce the gastric adverse effects associated with RIS by preventing its decomposition in the acidic condition of stomach. The newly developed microfluidic device for drug release testing may find applications in screening novel drugs and delivery systems.

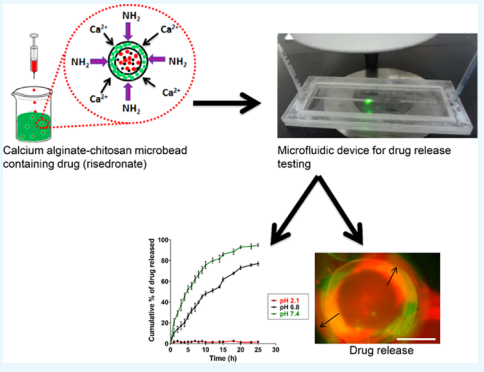

1. INTRODUCTION

There has been a noticeable progress in the recent years on environmentally sensitive hydrogels.[1] With specific alterations in environmental conditions, smart hydrogels modify their morphology and porosity.[2] Hydrogels made from alginate (ALG) have several rare properties, which enables their use for entrapment or delivery of a wide range of therapeutic interventions, cells, or proteins.[3] In recent years, stimuli-responsive hydrogels that swell or shrink extremely with even minor transitions in the experimental conditions have received greater attention.[4,5] Several reports demonstrated the effect of chemical as well as physical stimuli on hydrogel.[6−8] Due to unique properties, hydrogels have generated great importance for their application in bio-sensing and drug delivery.[9]

ALG is produced on a large scale from brown seaweed and used extensively in foods, pharmaceuticals, and regenerative medicines.[10] ALG can form hydrogel by cross-linking with divalent cations (e.g., calcium, barium, strontium, and zinc), and this important characteristic of ALG allows its applications in drug delivery systems (Scheme 1).[11] ALG is used extensively in the pharmaceutical industry due to its mucoadhesive property.[12] ALG contains blocks of (1,4)-linked β-D-mannuronate (M) and α-L-guluronate (G) residues. ALG with high M content was reported to be immunogenic and potent in inducing cytokine production as compared with G in some studies.[13] Therefore, it is noteworthy to mention here that strict isolation and purification protocols are required to ensure minimal concentrations of endotoxins and immunogenic residues.[14] On the other hand, chitosan (CHT) is a biocompatible polysaccharide produced from chitin and used extensively for cell culture and drug delivery studies.[15] CHT has gained immense attention due to its antimicrobial, wound healing,[16] anti-inflammatory,[17] antihypertensive,[18] and tissue regeneration properties.[19] The stability of hydrogel formed from ALG can be improved further by cross-linking of ALG with CHT.[11] In recent years, hydrogel

Received: October 17, 2019
Accepted: December 16, 2019
Published: December 30, 2019

DOI: 10.1021/acsomega.9b03464
ACS Omega 2020, 5, 758−765

Scheme 1. Cross-linking Mechanism of NaALG with Calcium Ions

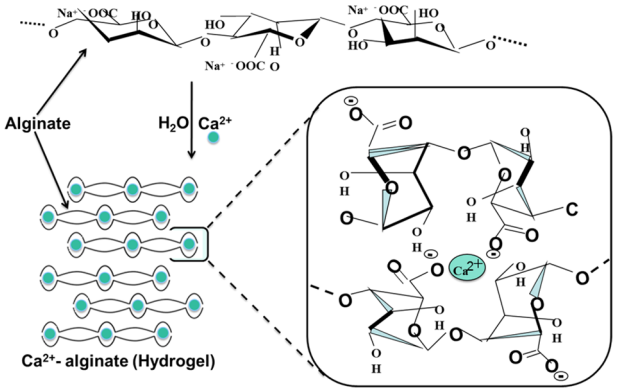

formed from ALG and CHT complex is useful in pharmaceutical applications, especially in controlled drug delivery systems.[20]

Risedronate (RIS), a third-generation bisphosphonate, is an antiresorptive drug preferred mainly for osteoporosis.[21] RIS has been shown to increase or maintain bone density and reduce the fracture.[22] Despite the benefits of RIS in various bone diseases, the oral bioavailability of this drug molecule is below one percentage because of low absorption due to ionization and hydrophilic nature of RIS, which inhibits transcellular transportation through the intestinal epithelium.[23,24] Additionally, RIS form complexes divalent cations with food, which further reduces its oral bioavailability.[25] Further, oral administration of RIS is also associated with gastrointestinal adverse effects.[26] Therefore, to improve the oral bioavailability and to prevent the adverse effects associated with RIS, it must be taken during a fasting condition while staying in an upstanding position for 30 min.[27,28]

Here, we report pH responsive calcium alginate (CaALG)−CHT based microbeads containing RIS. These microbeads were designed for programmed RIS release, i.e., no release in stomach (range pH 1−2.5)[29] to prevent gastric degradation of RIS and then sustained RIS release in the upper gastrointestinal tract (range pH 6.6−7.5),[29] where RIS has the higher absorption rate. The rationale of this study was linked to the aim of improving RIS therapeutic effectiveness by preventing the decomposition of RIS in the acidic condition of stomach as well as reducing its gastric side effects by coating with pH responsive CaALG−CHT-based microbeads that are resistant to the acidic environment of the stomach. Experimentally, we observed that presence of water in the hydrogel is extremely important for swelling as well as for the pH level to be sensed. Therefore, in this work, we first investigate the effect of this threshold water level in the initial dry hydrogel microbead. We considered a core−shell structure of sodium alginate (NaALG) and calcium chloride ($CaCl_2$) in spherical microbeads.

Microfluidic platforms allow researchers to carry out cell-based assays in small volume.[30] Windbergs and Weitz reported a drug dissolution microfluidic chip for multiparticulate drug delivery systems, which allows simultaneous analysis of the drug concentration present in the dissolution medium.[31] Here, we report a novel microfluidic device for drug release testing to study the programmed release of RIS encapsulated in pH responsive CaALG−CHT microbeads.

2. RESULTS AND DISCUSSION

Figure 1a shows the threshold water (wt %) needed to initiate ionic diffusion in the hydrogel. The threshold water concentration increases with $CaCl_2$, indicating the gel formation equilibrium state being dependent on the number of Ca^{2+} ions. CaALG microbeads of various diameters were prepared by different $CaCl_2$ concentrations and hypodermic syringes of different diameters (0.32, 0.64, 1.02, to 1.28 mm). We observed differences in the swelling rate of CaALG microbeads made by using various concentrations of $CaCl_2$ content as well as different syringes with varying diameter. The swelling profile of CaALG microbeads prepared with 10−15 M $CaCl_2$ concentration and a hypodermic syringe with diameter 1.28 mm showed a substantial increase in the swelling rate at pH 8 as compared with the CaALG microbeads prepared with hypodermic syringes with diameters of 0.32, 0.64, and 1.02 mm, respectively. It is noteworthy to mention that this swelling rate and disintegration of CaALG microbeads at higher pH is due to the ionic exchange between Ca^{2+} linked to carboxylic groups of the CaALG microbeads and Na^+ (present in the at pH 8 phosphate buffer).[11] These results indicate that by optimizing the CaALG microbead size, concentration of the Ca^{2+} ions, it is possible to design a target diffusion rate of biomolecules across the shell of the bead in a specific range of pH condition.

Figure 1b shows the nonlinear and hysteretic nature of electrical conductivity as a function of the applied bias voltage. The preweighed dry CaALG microbeads prepared by using different $CaCl_2$ concentrations and a hypodermic syringe with diameter 1.28 mm were immersed in different pH solutions and the change in conductivity was studied at a different voltage till the microbeads showed different conductivity, indicating instability in terms of ion transport. In the forward (FV) and

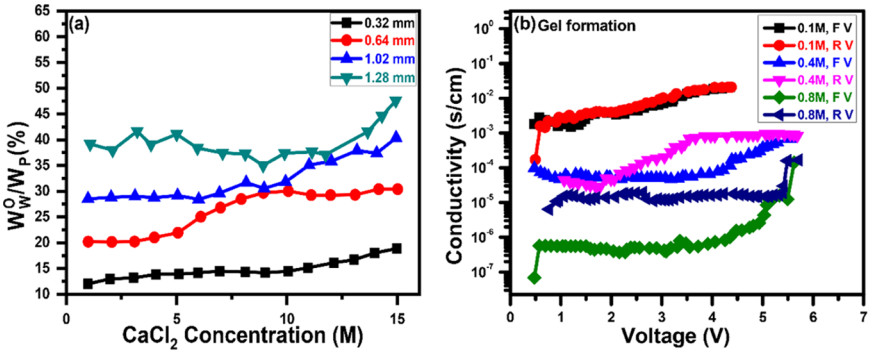

Figure 1. (a) Effect of initial core diameter on the threshold water concentration in the CaALG microbeads for various $CaCl_2$ concentrations, (b) electrical conductivity (FV and RV) as a function of bias voltage during gel formation.

DOI: 10.1021/acsomega.9b03464
ACS Omega 2020, 5, 758−765

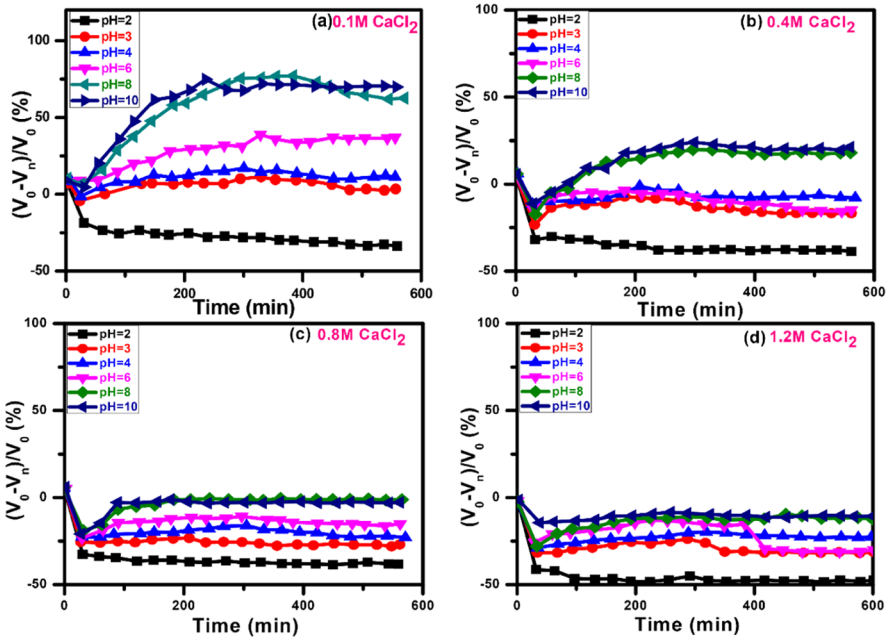

Figure 2. Percentage change in the volume due to swelling/shrinking for various pH values of the solvent and syringe diameter, 1.28 mm for (a) 0.1 M, (b) 0.4 M, (c) 0.8 M, and (d) 1.2 M $CaCl_2$ shell in the presence of electric potential and pH imbalance.

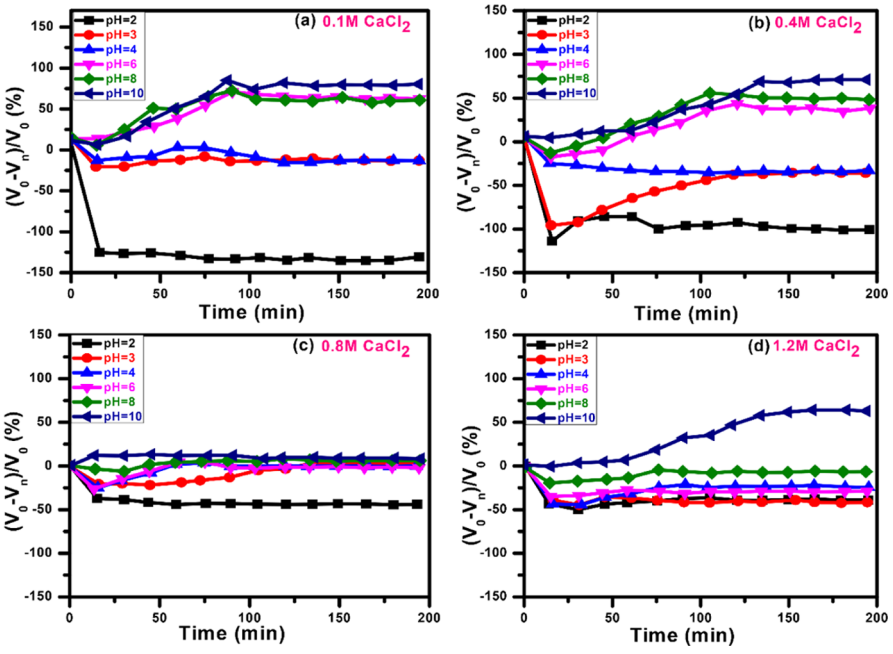

Figure 3. Percentage change in the volume due to swelling/shrinking for various pH values of the solvent and syringe diameter of 0.32 mm for (a) 0.1 M, (b) 0.4 M, (c) 0.8 M, and (d) 1.2 M $CaCl_2$ shells.

reverse (RV) sweeps of bias voltage, the conductivities show a nearly linear behavior when Ca^{2+} ion concentration is small (0.1 M). Hysteresis loop becomes large as the Ca^{2+} ion concentration increases. These results indicate different paths of phase transition in the process of Ca^{2+} ions subjected to different electric potential. The phases are not fully recovered when the Ca^{2+} ion concentration is large (0.8 M) even after the electric potential is removed. In this case, the conductivity increases by 1 order of magnitude after one full cycle, which indicates that the conductive paths in the network are formed and stabilized under the application of the electric potential. This understanding can be further applied to designing electrical stimuli-dependent diffusion (uptake or release) of biomolecules to and from the CaALG microbeads.

The swelling/shrinking profile of CaALG microbeads prepared with different (0.1, 0.4, 0.8, and 1.2 M) $CaCl_2$ concentrations and a hypodermic syringe with diameter 1.28 mm at various pH (2, 3, 4, 6, 8, and 10) conditions is shown in Figure 2. We exposed the CaALG microbeads to different pH (2, 3, 4, 6, 8, and 10) conditions abruptly and measured the volumetric changes. The relative change in the volume (V_n) of the CaALG microbeads relative to its initial volume (V_0) over time was measured when the CaALG microbeads were exposed to various pH conditions on the outside. A comparison of the

DOI: 10.1021/acsomega.9b03464
ACS Omega 2020, 5, 758−765

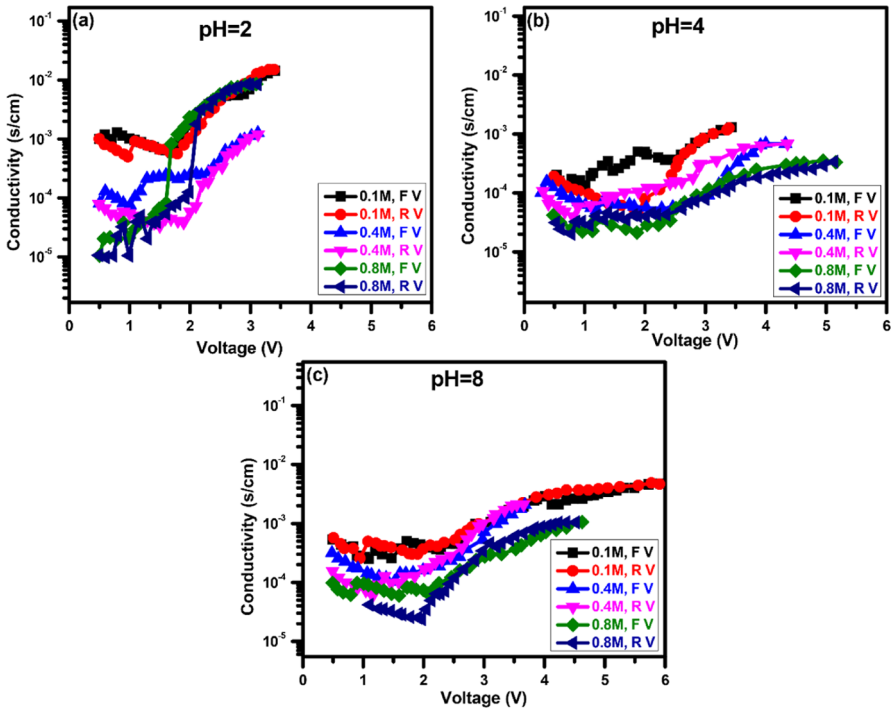

Figure 4. Conductivity as a function of the bias voltage at (a) pH = 2, (b) pH = 4, and (c) pH = 8.

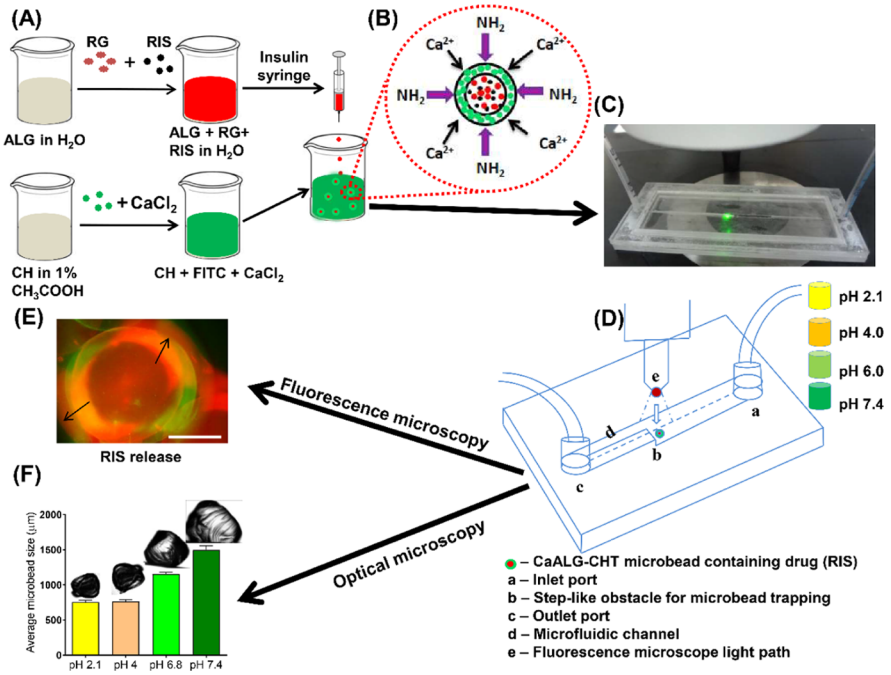

Figure 5. Synthesis and drug (RIS) release measurements of CaALG−CHT-based functionalized hydrogel core−shell microbead in a microfluidic device. (A) The CHT functional shell is optically labeled with the fluorescent marker fluorescein isothiocyanate (FITC); the core with the NaALG gel matrix containing RIS is optically labeled with RG. (B) Schematic representation of polyelectrolyte complex formation between CaALG−CHT. (C) Original photograph of the microfluidic device during assessment of RIS release in the microchannel. (D) Schematic representation of RIS release setup in the microfluidic device. (E) Fluorescence image of CaALG−CHT microbead containing RIS labeled with the fluorescent marker FITC (green) and RG (red). RIS release is exemplified by black arrows (scale bar: 200 μm). (F) Average size of the CaALG−CHT microbead. Bars represent means ± standard error of the mean (SEM) (n = 3). Representative optical microscopic images of CaALG−CHT microbead at different pH (2.1, 4, 6, and 7.4) conditions.

graphs in Figure 2a−d clearly indicates effectively a swelling characteristic when Ca^{2+} concentration in the shell is high (1.2 M, Figure 2d) for all pH (2, 3, 4, 6, 8, and 10) conditions, whereas the characteristic changes to volume shrinkage as the Ca^{2+} concentration reduces on the shell for pH greater than 3. An increase in the hydrogen bonding between the polymannuronate chains causes shrinkage of the CaALG microbeads. This implies that the net differential pressure across the CaALG

DOI: 10.1021/acsomega.9b03464
ACS Omega 2020, 5, 758−765

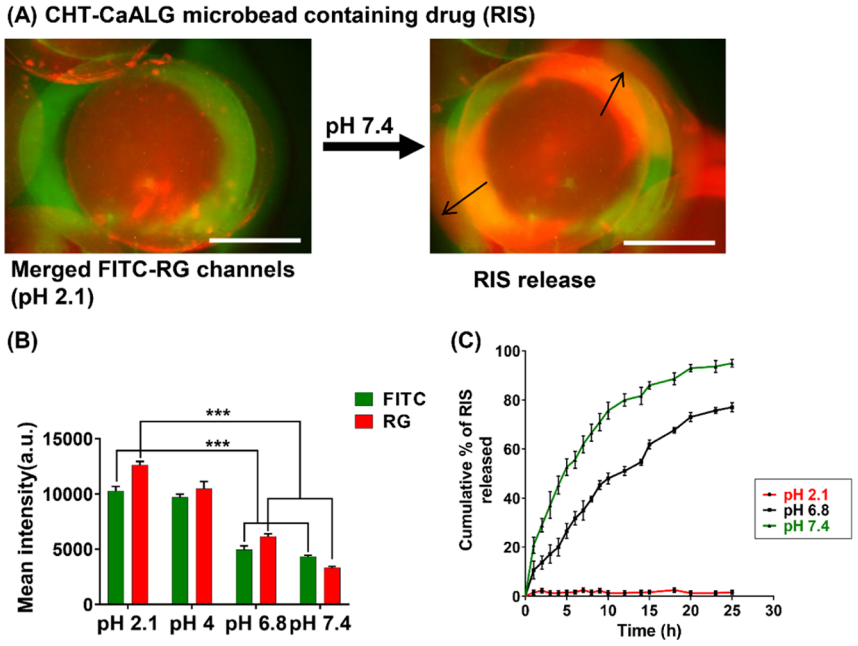

Figure 6. Release profiles of drug (RIS) from CaALG−CHT based microbead. CHT labeled with FITC (green) in the outer shell of the microbead and RG (red) labeled NaALG in the core for monitoring RIS release. (A) Representative images of CaALG−CHT based microbead loaded with RIS, at pH 2.1 and pH 7.4. RIS release is exemplified by black arrows (scale bar: 200 μm). (B) Fluorescence intensity for FITC and RG at various pH (2.1, 4, 6.8, and 7.4) conditions. Bars represent mean ± SEM (n = 3). ***P < 0.001 compared with pH 2.1, using unpaired student t-test. (C) Cumulative percentage of RIS release in a microfluidic channel over time from a CaALG−CHT based microbead. Bars represent mean ± SEM (n = 3).

microbeads shell (difference between the diffusive force and the cohesive force) increases in favor of the water molecules moving into the CaALG microbeads at pH > 3 for 0.1 M $CaCl_2$. In these CaALG microbeads, diffusion takes place for approximately the first 200 min due to a sudden pH imbalance, following which the volume becomes stable, which is the case for all cases of pH and Ca^{2+} concentration. As shown in Figure 2, at a pH of 6−7, the CaALG microbeads with a concentration slightly below 0.4 M $CaCl_2$ can result in good stability of the bead volume.

Similar results are shown for smaller CaALG microbeads prepared with 0.1, 0.4, 0.8, and 1.2 M $CaCl_2$ concentration and a hypodermic syringe with diameter 0.32 mm at various pH (2, 3, 4, 6, 8, and 10) conditions (Figure 3). The band of swelling and shrinkage has further reduced, and the volume is more stable for 0.8 M $CaCl_2$ at all pH of 4−8 (see Figure 3c). However, at higher pH conditions, due to the small size effect (smaller diameter of the CaALG microbeads), the diffusion rate appears to be lower than that in the case of larger CaALG microbead size (Figure 3).

Electrical conductivity of CaALG microbeads as a function of the voltage for pH = 2 is shown in Figure 4a. Here, an increasing molar concentration of $CaCl_2$ indicates increased thickness of the shell layer formed on the core of CaALG microbeads. The conductivity of CaALG microbeads prepared from 0.1 M $CaCl_2$ is greater than that of CaALG microbeads prepared from 0.4 and 0.8 M $CaCl_2$. For the 0.4 and 0.8 M $CaCl_2$ beads, hysteresis loop both during gel formation as well as during exposure at a pH of 2 is observed. During gel formation, no hysteresis loop is formed for 0.1 M $CaCl_2$ CaALG microbeads. Conductivity of CaALG microbeads as a function of the voltage at a pH of 4 and 8 is shown in Figure 4b,c, respectively. Increased molar concentrations of $CaCl_2$ clearly indicate increase in the thickness of the shell layer of the bead. It can be seen that the conductivity due to 0.8 M $CaCl_2$ is greater than the conductivity due to 0.4 M $CaCl_2$. $CaCl_2$ of 0.8 M concentration forms a hysteresis loop in both solutions of pH = 4 and 8. But at a pH of 4, higher the concentration of $CaCl_2$ is, higher is the conductivity. In contrast, at pH 8, a higher concentration of $CaCl_2$ showed lower conductivity and the hysteresis loop was not formed.

It is observed that for a concentration below 0.8 M $CaCl_2$ at pH = 8, the rate of change of conductivity over bias voltage increases, and at pH of 4, just an opposite trend is observed. Below the concentration of 0.8 M $CaCl_2$, the shell is thicker and that is why the conductivity drops. This may be attributed to the pH activated ion transport between CaALG microbeads and the solution. Moreover, we did not observe complete disintegration of CaALG microbeads, which indicates that the cross-linking of the CaALG microbeads was not changed at lower pH, as observed with high pH. This indicates that Ca^{2+} ions were not replaced effectively by H^+ ions. When the concentration of H^+ ion rises above a threshold value, the H^+ ions emigrate into the CaALG microbeads, which disturbs the inner electroneutrality of the microbeads. This consecutively leads to the outward flux of anions from the CaALG microbeads. The conductivity range widens for pH of 2, and it reduces as the pH crosses 6. For the extreme condition of pH = 2 and 0.8 M $CaCl_2$ (Figure 4a), a sharp transition in the phase can be seen with a hysteresis loop around 2 V. Around these transition states, by altering the voltage, it is possible to create electrical stimulation to change the electrical conductivity. A change in the electrical conductivity would produce ionic diffusion.

Figure 5A,B shows a schematic representation of fluorescently labeled CaALG−CHT microbeads and a possible mechanism of polyelectrolyte complex formation between CHT and ALG microbeads, containing RIS. In this study, we used a microfluidic device for enabling live optical and fluorescence imaging of the fluorescently labeled microbeads containing risedronate at different pH (2.1, 4, 6, and 7.4) conditions (Figure 5C,D). pH-dependent properties of the CaALG−CHT microbeads containing RIS were studied by using optical and fluorescence microscopy at different pH conditions inside the microfluidic

DOI: 10.1021/acsomega.9b03464
ACS Omega 2020, 5, 758−765

device (Figures 5E,F and 6A,B). CaALG−CHT microbeads containing RIS synthesized at pH 6 were exposed to pH 2.1 and 4; their size decreased from 1152 ± 15.58 to 756.28 ± 14.60 and 762.01 ± 15.72 μm, respectively (Figure 5F). This decrease in CaALG−CHT microbead size can be explained by the coiling of CHT and ALG chains at the cross-linking points. The increased size of CaALG−CHT microbeads at pH of 7.4 indicates that the swelling of the CaALG−CHT microbeads was enhanced due to ionization of carboxylic acid groups in ALG, which resulted in Donnan osmotic swelling of the CaALG−CHT microbeads.

Figure 6A shows the representative fluorescence images of CaALG−CHT microbeads containing RIS at pH 2.1 and 7.4. The RIS release was clearly observed at pH 7.4. We analyzed the mean fluorescence intensity of fluorescein isothiocyanate isomer I (FITC), rhodamine 6G (RG) observed for CaALG−CHT microbeads containing RIS at different pH (2.1, 4, 6.8, and 7.4) conditions. The mean fluorescence intensity of FITC and RG observed at pH 6.8 and 7.4 for CaALG−CHT microbeads containing RIS was significantly ($P < 0.001$) lower as compared to that for pH 2.1 (Figure 6B). This may be attributed to the disintegration of CaALG−CHT microbeads at pH 6.8 and 7.4 and release of RIS. We coated ALG with CHT to prevent the burst release of RIS after immediate disintegration of CaALG microbeads at pH 7.4. As shown in Figure 6C, at lower pH 2.1, the RIS release from CHT−CaALG microbeads was minimal due to the inability of the acidic buffer medium to penetrate the CaALG−CHT microbead. In contrast, the initial pronounced release of the RIS at pH 6.8 and 7.4, followed by sustained release after 10 h might be due to these factors: (i) initially, Ca^{2+} ions present in the polymannuronate units of ALG are exchanged with Na^{+} ions present in the buffer solution,[32] which causes chain relaxation and enhanced swelling and RIS release; (ii) further, Ca^{2+} ions bind with the −COO− group of the polyglucuronate units and thus form the tight egg-box structure, which also starts to exchange with Na^{+} ions in the buffer medium because polyglucuronate sequences have a strong autocooperative binding of Ca^{2+} ions.

We demonstrated the pH-sensitive diffusion through the CaALG−CHT based microbeads by considering the problem of releasing an osteoporosis drug RIS.[24] It is noteworthy to mention that the coating of CaALG−RIS with CHT considerably reduced RIS release in acidic pH due to shrinkage of the CaALG−CHT beads. The probable reason is that electrostatic interaction between the amino group of CHT and carboxyl groups of the ALG generated a compact surface layer that reduced fluid diffusion and erosion of the pH-sensitive microbeads. The swelling of the CaALG−CHT beads increased dramatically at pH 6.8 and 7.4, which resulted in initial burst release of RIS followed by a sustained release over an extended period of time up to 24 h. Slow release of drug is an important factor to be considered in CaALG−CHT based microbeads. Therapies for osteoporosis and Paget's disease can benefit from controlled release of the RIS for extended delivery of this drug to the duodenum and jejunum parts of the intestine.[33] Controlled RIS release should allow an improvement in bioavailability, thus allowing a lowering of the total dose of RIS. The rationale of this study was linked to the aim of improving RIS therapeutic effectiveness by preventing the decomposition of RIS in the acidic condition of stomach as well as reducing its gastric side effects by coating with pH responsive CaALG−CHT based microbeads that are resistant to the acidic environment of the stomach. Finally, we also reported a newly developed microfluidic device, which is used as a tool to evaluate the in vitro RIS release pattern from developed pH responsive CaALG−CHT based microbeads. The microfluidic device described here may have substantial potential for use in analytical and diagnostic assays as well as in drug-screening applications. The present study may be used as a baseline for future investigations in developing a microfluidic device to study drug diffusion from novel drug delivery systems.

4. CONCLUSIONS

In this study, we reported the pH-dependent swelling and threshold water dependence on the core−shell structure of CaALG hydrogel microbeads. We also demonstrated that a sustained release RIS delivery system can be formulated by coating of pH-sensitive CaALG-based microbeads, with CHT. We also reported a newly developed microfluidic device for drug release testing that could ultimately replace animal models. This microfluidic device might have a potential role in the overall drug discovery process to predict drug efficacy and safety.

5. MATERIAL AND METHODS

5.1. Materials. RIS was procured from Fleming Laboratories (Hyderabad, India). NaALG (viscosity: 4−12 cP), $CaCl_2$, CHT (viscosity: 5−200 mPa s), acetic acid, FITC, and RG were purchased from Sigma (Bengaluru, India).

5.2. Fabrication of Microbeads. CaALG microbeads were fabricated by the gelation method, as reported by Segale et al.,[11] with modifications. Briefly, NaALG was mixed in high pure water at a concentration of 3% (w/v). With the help of a micropipettor, this aqueous solution of NaALG was filled in an insulin syringe needle with a gauge size 31 and added drop wise to separate glass beakers containing 0.1, 0.4, 0.8, and 1.2 M of $CaCl_2$ aqueous solution kept under pH 6 with continuous stirring (500 rpm). After 20 min, the microbeads were collected, followed by washing with deionized water and then dried at 35 °C overnight.

5.3. Electrical Conductivity Measurement. Before electrical conductivity analysis, the dried microbeads of CaALG hydrogel were swollen in deionized water. The electrical conductivity of the fabricated CaALG hydrogel microbeads was estimated by using the circuit current for various direct current (DC) bias voltages applied across the microbead. An electrical circuit with a known resistor in series with the bead sample was connected to a data acquisition system, and DC voltage was applied. Bulk resistivity of the CaALG microbeads was determined by applying the equation reported by Yang et al.[34]

5.4. Fabrication of RIS-Encapsulated CaALG−CHT Microbeads. First, 10 mL of NaALG solution (3% w/v) was added in deionized water. Secondly, to 10 mL of NaALG solution, 1 mL of RIS solution (0.1% w/v) was added drop wise with continuous stirring (1000 rpm). With the help of a micropipettor, NaALG solution containing RIS was filled in an insulin syringe needle with a gauge size 31 and added drop wise to separate glass beakers containing gelation medium kept under pH 6 with continuous stirring (500 rpm). The resulting microbeads were collected and transferred into a CHT solution (1% w/v), which was prepared in acetic acid (2%). After 15 min, the microbeads were collected, followed by washing with highly deionized water and then dried at 35 °C overnight.

5.5. Fabrication of Fluorescently Labeled RIS-Encapsulated CaALG−CHT Microbeads. First, 10 mL of NaALG solution (3% w/v) was added in deionized water. For FITC-loaded NaALG, 3 mg of FITC was dissolved in 200 μL of

DOI: 10.1021/acsomega.9b03464
ACS Omega 2020, 5, 758−765

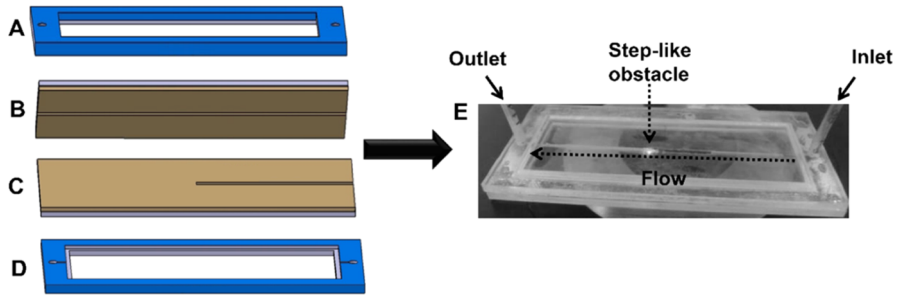

Figure 7. Microfluidic device to study drug delivery systems in vitro. (A–D) Schematic view of the microfluidic device, (A) acrylic top plate with microvalve, (B) PDMS-coated top glass plate with a microchannel, (C) PDMS-coated bottom glass plate with a microchannel containing a steplike obstacle, (D) acrylic bottom plate with a microvalve, (E) picture of a fabricated microfluidic device with fluidic connections.

dimethylformamide and then added into the NaALG solution under gentle stirring. These procedures were protected from light due to sensitivity of FITC to light. Second, to 10 mL of NaALG solution, 1 mL of RIS solution (0.1% w/v) was added drop wise with continuous stirring (1000 rpm). With the help of a micropipettor, NaALG solution containing RIS was filled in an insulin syringe needle with a gauge size 31 and added drop wise to separate glass beakers containing gelation medium kept under pH 6 with continuous stirring (500 rpm). The resulting microbeads were collected and transferred into a CHT solution (1% w/v). After 15 min, the microbeads were collected, followed by washing with deionized water. FITC-labeled RIS-loaded ALG hydrogels were further coated with CHT labeled with RG. These fluorescence-labeled microbeads were examined by using optical and fluorescence microscopy (Axiovert 200, Carl Zeiss MicroImaging GmbH, Germany).[35]

5.6. Microfluidic Device. Figure 7 shows the schematic illustration of the microfluidic device, which was used as a tool to evaluate the in vitro RIS release pattern from developed pH responsive CaALG–CHT-based microbeads. Briefly, our microfluidic device contains single inlet and outlet ports. The top and bottom layers of the microfluidic device containing microvalves were fabricated from transparent acrylic plates. The two middle layers were fabricated by using poly-(dimethylsiloxane) (PDMS)-coated glass (22 mm × 60 mm^2, thickness, 2 mm) with a single straight microchannel containing a steplike barrier design used to restrict the mobility of the microbeads at the sample detection zone (Figure 1C). For fluorescence microscopy, single fluorescently labeled CaALG–CHT-based microbeads containing RIS were placed in the sample detection zone by flowing through the inlet port with ultrapure water.

5.7. In Vitro Drug Release. For investigation of drug release, single CaALG–CHT-based microbeads containing RIS were placed in a microfluidic device (Figure 1). At different time intervals, the release of RIS from the microbeads at different pH conditions was determined by using a StellarNet EPP2000 concave grating UV–vis spectrophotometer at 262 nm.[36] This process was carried out in triplicate at ambient temperature.

5.8. Statistical Analysis. Data is presented as mean ± SEM. Unpaired Student's *t* tests were carried out using GraphPad PRISM 8 software, (GraphPad Software, La Jolla, CA). The significance is indicated using asterisks; $P < 0.001$(***).

AUTHOR INFORMATION

Corresponding Authors

*E-mail: deepak_kumarkhajuria@yahoo.co.in (D.K.K.).
*E-mail: roymahapatra@iisc.ac.in (D.R.M.).

ORCID

Deepak Kumar Khajuria: 0000-0002-3737-8504

Author Contributions

§R.V. and M.K.P. have contributed equally to this work.

Notes

The authors declare no competing financial interest.

ACKNOWLEDGMENTS

The authors are grateful to the experimental assistance of Harsh Vardhan (Research Staff) from Laboratory for Integrative Multiscale Engineering Materials and Systems, Department of Aerospace Engineering, Indian Institute of Science. D.R.M. thankfully acknowledges financial support through the project IDC-Water under the 2+2 program of the Indo-German Science and Technology Centre (IGSTC).

REFERENCES

(1) Ahmed, E. M. Hydrogel: Preparation, characterization, and applications: A review. *J. Adv. Res.* **2015**, *6*, 105–121.
(2) Rizwan, M.; Yahya, R.; Hassan, A.; Yar, M.; Azzahari, D. A.; Selvanathan, V.; Sonsudin, F.; Abouloula, N. C. pH Sensitive Hydrogels in Drug Delivery: Brief History, Properties, Swelling, and Release Mechanism, Material Selection and Applications. *Polymers* **2017**, *9*, 137.
(3) García-Torres, J.; Gispert, C.; Gomez, E.; Valles, E. Alginate electrodeposition onto three-dimensional porous Co-Ni films as drug delivery platforms. *Phys. Chem. Chem. Phys.* **2015**, *17*, 1630–1636.
(4) Yu, L.; Grist, S. M.; Nasseri, S. S.; Cheng, E.; Hwang, Y. C. E.; Ni, C.; Cheung, K. C. Core-shell hydrogel beads with extracellular matrix for tumor spheroid formation. *Biomicrofluidics.* **2015**, *9*, No. 024118.
(5) Doring, A.; Birnbaum, W.; Kuckling, D. Responsive hydrogels - structurally and dimensionally optimized smart frameworks for applications in catalysis, micro-system technology and material science. *Chem. Soc. Rev.* **2013**, *42*, 7391–7420.
(6) Pandeeswar, M.; Senanayak, S. P.; Narayan, K. S.; Govindaraju, T. Multi-Stimuli-Responsive Charge-Transfer Hydrogel for Room-Temperature Organic Ferroelectric Thin-Film Devices. *J. Am. Chem. Soc.* **2016**, *138*, 8259–8268.
(7) Tavakol, M.; Vasheghani-Farahani, E.; Hashemi-Najafabadi, S. The effect of polymer and CaCl2 concentrations on the sulfasalazine release from alginate-N,O-carboxymethyl chitosan beads. *Prog. Biomater.* **2013**, *2*, 10.
(8) Yamanaka, M.; Haraya, N.; Yamamichi, S. Chemical stimuli-responsive supramolecular hydrogel from amphiphilic tris-urea. *Chem. - Asian J.* **2011**, *6*, 1022–1025.
(9) Shen, X.; Shamshina, J. L.; Berton, P.; Gurau, G.; Rogers, R. D. Hydrogels based on cellulose and chitin: fabrication, properties, and applications. *Green Chem.* **2016**, *18*, 53–75.
(10) Hecht, H.; Srebnik, S. Structural Characterization of Sodium Alginate and Calcium Alginate. *Biomacromolecules* **2016**, *17*, 2160–2167.

DOI: 10.1021/acsomega.9b03464
ACS Omega 2020, 5, 758–765

(11) Segale, L.; Giovannelli, L.; Mannina, P.; Pattarino, F. Calcium Alginate and Calcium Alginate-Chitosan Beads Containing Celecoxib Solubilized in a Self-Emulsifying Phase. *Scientifica* **2016**, *2016*, 8.
(12) Szekalska, M.; Puciowska, A.; Szymaska, E.; Ciosek, P.; Winnicka, K. Alginate: Current Use and Future Perspectives in Pharmaceutical and Biomedical Applications. *Int. J. Polym. Sci.* **2016**, *2016*, 17.
(13) Lee, K. Y.; Mooney, D. J. Alginate: properties and biomedical applications. *Prog. Polym. Sci.* **2012**, *37*, 106−126.
(14) Sosnik, A. Alginate Particles as Platform for Drug Delivery by the Oral Route: State-of-the-Art. *ISRN Pharm.* **2014**, *2014*, No. 926157.
(15) Cheung, R. C. F.; Ng, T. B.; Wong, J. H.; Chan, W. Y. Chitosan: An Update on Potential Biomedical and Pharmaceutical Applications. *Mar. Drugs* **2015**, *13*, 5156−5186.
(16) Dai, T.; Tanaka, M.; Huang, Y.-Y.; Hamblin, M. R. Chitosan preparations for wounds and burns: antimicrobial and wound-healing effects. *Expert Rev. Anti-Infect. Ther.* **2011**, *9*, 857−879.
(17) Davydova, V. N.; Kalitnik, A. A.; Markov, P. A.; Volod'ko, A. V.; Popov, S. V.; Ermak, I. M. Cytokine-inducing and anti-inflammatory activity of chitosan and its low-molecular derivative. *Appl. Biochem. Microbiol.* **2016**, *52*, 476−482.
(18) Park, S. H.; Dutta, N. K.; Baek, M. W.; Kim, D. J.; Na, Y. R.; Seok, S. H.; Lee, B. H.; Cho, J. E.; Cho, G. S.; Park, J. H. NaCl plus chitosan as a dietary salt to prevent the development of hypertension in spontaneously hypertensive rats. *J. Vet. Sci.* **2009**, *10*, 141−146.
(19) Hurt, A. P.; Kotha, A. K.; Trivedi, V.; Coleman, N. J. Bioactivity, biocompatibility and antimicrobial properties of a chitosan-mineral composite for periodontal tissue regeneration. *Polímeros* **2015**, *25*, 311−316.
(20) Li, X.; Du, P.; Liu, P. Layer-by-layer polyelectrolyte complex coated poly(methacrylic acid) nanogels as a drug delivery system for controlled release: structural effects. *RSC Adv.* **2014**, *4*, 56323−56331.
(21) Krishnan, S.; Pandian, S.; Kumar S, A. Effect of Bisphosphonates on Orthodontic Tooth Movement—An Update. *J. Clin. Diagn. Res.* **2015**, *9*, ZE01−ZE05.
(22) Gallagher, J. C.; Tella, S. H. Prevention and treatment of postmenopausal osteoporosis. *J. Steroid Biochem. Mol. Biol.* **2014**, *142*, 155−170.
(23) Wright, N. C.; Looker, A. C.; Saag, K. G.; Curtis, J. R.; Delzell, E. S.; Randall, S.; Dawson-Hughes, B. The Recent Prevalence of Osteoporosis and Low Bone Mass in the United States Based on Bone Mineral Density at the Femoral Neck or Lumbar Spine. *J. Bone Miner. Res.* **2014**, *29*, 2520−2526.
(24) Dalle Carbonare, L.; Zanatta, M.; Gasparetto, A.; Valenti, M. T. Safety and tolerability of zoledronic acid and other bisphosphonates in osteoporosis management. *Drug, Healthcare Patient Saf.* **2010**, *2*, 121−137.
(25) Ezra, A.; Golomb, G. Administration routes and delivery systems of bisphosphonates for the treatment of bone resorption. *Adv. Drug Delivery Rev.* **2000**, *42*, 175−195.
(26) Bock, O.; Boerst, H.; Thomasius, F. E.; Degner, C.; Stephan-Oelkers, M.; Valentine, S. M.; Felsenberg, D. Common musculoskeletal adverse effects of oral treatment with once weekly alendronate and risedronate in patients with osteoporosis and ways for their prevention. *J. Musculoskeletal Neuronal Interact.* **2007**, *7*, 144−148.
(27) Poole, K. E.; Compston, J. E. Bisphosphonates in the treatment of osteoporosis. *BMJ* **2012**, *344*, No. e3211.
(28) Abrahamsen, B. Adverse Effects of Bisphosphonates. *Calcif. Tissue Int.* **2010**, *86*, 421−435.
(29) Evans, D. F.; Pye, G.; Bramley, R.; Clark, A. G.; Dyson, T. J.; Hardcastle, J. D. Measurement of gastrointestinal pH profiles in normal ambulant human subjects. *Gut* **1988**, *29*, 1035−1041.
(30) Eduati, F.; Utharala, R.; Madhavan, D.; Neumann, U. P.; Longerich, T.; Cramer, T.; Saez-Rodriguez, J.; Merten, C. A. A microfluidics platform for combinatorial drug screening on cancer biopsies. *Nat. Commun.* **2018**, *9*, No. 2434.
(31) Windbergs, M.; Weitz, D. A. Drug dissolution chip (DDC): a microfluidic approach for drug release. *Small* **2011**, *7*, 3011−3015.
(32) Basu, S. K.; Rajendran, A. Studies in the development of nateglinide loaded calcium alginate and chitosan coated calcium alginate beads. *Chem. Pharm. Bull.* **2008**, *56*, 1077−1084.
(33) Pazianas, M.; Abrahamsen, B.; Ferrari, S.; Russell, R. G. Eliminating the need for fasting with oral administration of bisphosphonates. *Ther. Clin. Risk Manage.* **2013**, *9*, 395−402.
(34) Yang, J.; Choe, G.; Yang, S.; Jo, H.; Lee, J. Y. Polypyrrole-incorporated conductive hyaluronic acid hydrogels. *Biomater. Res.* **2016**, *20*, 31.
(35) Khajuria, D. K.; Konnur, M. C.; Vasireddi, R.; Mahapatra, D. R. Photonic monitoring of chitosan nanostructured alginate microcapsules for drug release. *Proc. SPIE* **2015**, *9303*, No. 93033V.
(36) Sahana, H.; Khajuria, D. K.; Razdan, R.; Mahapatra, D. R.; Bhat, M. R.; Suresh, S.; Rao, R. R.; Mariappan, L. Improvement in bone properties by using risedronate adsorbed hydroxyapatite novel nanoparticle based formulation in a rat model of osteoporosis. *J. Biomed. Nanotechnol.* **2013**, *9*, 193−201.

DOI: 10.1021/acsomega.9b03464
ACS Omega 2020, 5, 758−765